HHS Public Access

Author manuscript

J Comp Neurol. Author manuscript; available in PMC 2019 January 01.

Published in final edited form as:

J Comp Neurol. 2019 January 01; 527(1): 328–344. doi:10.1002/cne.24377.

Distribution and diversity of intrinsically photosensitive retinal ganglion cells in tree shrew

Elizabeth N. Johnson[1,2], **Teleza Westbrook**[1], **Rod Shayesteh**[1], **Emily L. Chen**[1], **Joseph W. Schumacher**[3], **David Fitzpatrick**[3], and **Greg D. Field**[1,*]

[1]Neurobiology Department, Duke University School of Medicine, Durham, North Carolina

[2]Wharton Neuroscience Initiative, The Wharton School, University of Pennsylvania, Philadelphia, Pennsylvania

[3]Max Planck Florida Institute for Neuroscience, Jupiter, Florida

Abstract

Intrinsically photosensitive retinal ganglion cells (ipRGCs) mediate the pupillary light reflex, circadian entrainment, and may contribute to luminance and color perception. The diversity of ipRGCs varies from rodents to primates, suggesting differences in their contributions to retinal output. To further understand the variability in their organization and diversity across species, we used immunohistochemical methods to examine ipRGCs in tree shrew (*Tupaia belangeri*). Tree shrews share membership in the same clade, or evolutionary branch, as rodents and primates. They are highly visual, diurnal animals with a cone-dominated retina and a geniculo-cortical organization resembling that of primates. We identified cells with morphological similarities to M1 and M2 cells described previously in rodents and primates. M1-like cells typically had somas in the ganglion cell layer, with 23% displaced to the inner nuclear layer (INL). However, unlike M1 cells, they had bistratified dendritic fields ramifying in S1 and S5 that collectively tiled space. M2-like cells had dendritic fields restricted to S5 that were smaller and more densely branching. A novel third type of melanopsin immunopositive cell was identified. These cells had somata exclusively in the INL and monostratified dendritic fields restricted to S1 that tiled space. Surprisingly, these cells immunolabeled for tyrosine hydroxylase, a key component in dopamine synthesis. These cells immunolabeled for an RGC marker, not amacrine cell markers, suggesting that they are dopaminergic ipRGCs. We found no evidence for M4 or M5 ipRGCs, described previously in rodents. These results identify some organizational features of the ipRGC system that are canonical versus species-specific.

Introduction

Intrinsically photosensitive retinal ganglion cells (ipRGCS) mediate the critical function of entraining circadian-dependent biological processes to the day/night cycle of Earth (Berson,

*corresponding author: field@neuro.duke.edu.

Author Contributions. E.N.J, D.F. and G.D.F. conceived and designed the experiments; J.S. and G.D.F. harvested retinas; T.W., R.S., and E.L.C. processed retinas for immunohistochemistry and captured images. E.N.J, T.W., R.S., E.L.C. and G.D.F. analyzed images. E.N.J. and G.D.F. wrote the manuscript.

Dunn, & Takao, 2002). The defining characteristic of these RGCs is their expression of melanopsin, which endows them with the ability to respond to light in the absence of rod or cone-mediated synaptic input (Berson et al., 2002; Schmidt & Kofuji, 2011; Sand, Schmidt, & Kofuji, 2012). They also drive key functions such as the pupillary light reflex (Lucas et al., 2003; Spitschan, Jain, Brainard, & Aguirre, 2014), and they likely contribute to color perception (Dacey et al., 2005) and spatial vision (Ecker et al., 2010; Sonoda & Schmidt, 2016; Allen, Storchi, Martial, Bedford, & Lucas, 2017). To support these diverse functions, ipRGC are comprised of different subtypes with axons that project to diverse brain areas including the lateral geniculate nucleus, suprachiasmatic nucleus, superior colliculus, olivary pretectal nucleus, intergeniculate leaflet, and medial amygdala (Hattar, Liao, Takao, Berson, & Yau, 2002; Hattar et al., 2006; Morin, Blanchard, & Provencio, 2003; Dacey et al., 2005; Ecker et al., 2010; Hannibal et al., 2014). Recent work to define the anatomical diversity of these cells has revealed substantial differences across mammals. For example, in mice and rats, ipRGCs are composed of at least five subtypes, while in old and new world primates they may be restricted to two subtypes (Viney et al., 2007; Schmidt & Kofuji, 2009; Ecker et al., 2010; Zhao, Stafford, Godin, King, & Wong, 2014; Jusuf, Lee, Hannibal, & Grunert, 2007; Reifler et al., 2015; Liao et al., 2016; Nasir-Ahmad, Lee, Martin, & Grünert, 2017). This raises the possibility that different mammalian species are utilizing ipRGCs to serve different functions and/or that the manner in which ipRGCs mediate a given function varies across species. A step toward resolving these possibilities is to determine the anatomical diversity of ipRGCs across a greater range of species.

To better understand ipRGC diversity within and across different mammals, we studied the retina of the tree shrew (*Tupaia belangeri*). These animals provide a contrasting and complementary perspective on ipRGCs from other previously studied species which primarily include rodents and primates (Kaas, 2008; Kaas, 2013). First, tree shrews exhibit a cone dominated retina: ~95% of photoreceptors are cones (Müller, Peichl, De Grip, Gery, & Korf, 1989; Petry, Erichsen, & Szél, 1993). Previous studies of ipRGCS have focused on rod-dominated retinas where the fraction of cones is 5–10% of photoreceptors (Szel et al., 1992; Szél, Röhlich, Caffé, & van Veen, 1996; Packer, Hendrickson, & Curcio, 1989; Curcio, Sloan, Packer, Hendrickson, & Kalina, 1987). Second, tree shrews exhibit profoundly diurnal behavior; foraging and other behaviors are suppressed rapidly in darkness. This suggests that ipRGC-mediated signaling may strongly modulate their behavioral state (Lazzerini Ospri, Prusky, & Hattar, 2017). Third, tree shrews have a unique evolutionary relationship to primates and rodents, the two most extensively studied animal orders for ipRGC structure and function. Specifically, tree shrews are an evolutionary intermediate between rodentia and primates, with all three belonging to the Euarchontoglires clade (Schmitz, Ohme, & Zischler, 2000; Waddell, Kishino, & Ota, 2001; Nie et al., 2008; Fan et al., 2013; Lin et al., 2014; Zhou, Sun, Xu, Yang, & Li, 2015). Fourth, tree shrews have an extensively laminated lateral geniculate nucleus and highly organized orientation-tuned columns in primary visual cortex, similar in many respects to primates (Conway & Schiller, 1983; Conley, Fitzpatrick, & Diamond, 1984; Fitzpatrick, 1996; Van Hooser, Roy, Rhodes, Culp, & Fitzpatrick, 2013). However, they also have relatively lateralized eyes, like rodents. Finally, tree shrews are considered a ‘living fossil,’ with the fossil record indicating they have changed little over 35 million years (Li & Ni, 2016). Thus, determining the

diversity and prevalence of ipRGCs in tree shrews may provide unique insight into their evolution and function across mammals.

To determine the prevalence, diversity and organization of ipRGCs in tree shrew, we used immunohistochemical approaches to identify cells expressing melanopsin. These experiments revealed both common and novel features to ipRGCs in tree shrews compared to other mammals. For example, similar to primates and rodents, we identify at least two distinct ipRGC types. One type was monostratified in the vitreal side of the IPL (in sublayer 5) and had relatively densely branching dendrites, similar to M2 cells described in other species. The other type had bistratified dendrites at the outer and inner boundaries of the IPL (S1 and S5, respectively). These cells were regularly spaced and their dendritic fields approximately tiled the retina. These bistratified ipRGCs also exhibited a strong eccentricity-dependent gradient that peaked in the temporal retina just below the horizontal meridian, providing the first evidence for an *area centralis*-like region in tree shrew. We also identify a melanopsin-expressing cell type that may be unique to tree shrew. These cells were immunoreactive for melanopsin and tyrosine hydroxylase (TH). TH is a key component in dopamine synthesis and identifies dopaminergic cells in the retinae of other species. The dendrites of these cells were restricted to the outer portion of the IPL (S1) and they tiled space. Their density across the retina was higher than bistratified ipRGCs, and their density was more uniform across the retina. These cells failed to immunolabel for amacrine cell markers, but were immunolabeled by RBPMS, a specific and ubiquitous marker for RGCs (Rodriguez, de Sevilla Müller, & Brecha, 2014). Furthermore, TH immunoreactivity was limited to these cells. These results raise the possibility that dopamine release may be a function of ipRGCs in tree shrew and not of amacrine cells, differing from other mammals. An alternative possibility is that the tree shrew has intrinsically photosensitive amacrine cells. These results illustrate the extent to which melanopsin expression can be specialized to the environmental demands and behavioral needs of different species.

Methods

Animals and preparation of retinae

Retinas from nine adult tree shrews of both sexes were used. Some animals were euthanized following terminal experiments in which a cranial window was introduced to image primary visual cortex (Lee, Huang, & Fitzpatrick, 2016). Eyes from these animals were enucleated after perfusing the animal with either 2% or 4% PFA followed by a rinse of phosphate buffered saline (PBS, pH 7.4). Eyes were stored at 4°C in PBS+0.02% NaAzide until dissection. Other animals were acutely used and eyes were enucleated immediately following an overdose with Nembutal and decapitation (200 mg/kg). Hemisected eyes were then fixed for 30–60 mins in either 2% or 4% PFA. Following fixation, retinas were rinsed and stored in PBS+0.02% NaAzide. Fixed and unfixed eyes were hemisected by making an incision between the equator and ora serrata. The front half of the eye was removed with the lens. Vitreous was then peeled away from the retina. For whole mount retina, the sclera, choroid and pigment epithelium were removed and segments of retina were cut for immunolabeling. For retinal slices, eyecups were cryoprotected overnight immediately

following removal of the cornea and iris at 4°C in PBS with 30% sucrose. Eyecups were then frozen in TFM, sectioned at 20 μm thickness, and thaw-mounted onto Superfrost Plus Gold slides. Mounted slices were stored at −80°C until immunolabeling. Data displayed in Figs, 1–8 was collected from 9, 2, 2, 4, 2, 2, 1, 2 animals, respectively.

Retinas from two adult Nile rats (*Arvicanthis niloticus*), of both sexes were used. The eyes were generously provided by Dr. K.C. Hayes at Brandeis University. Animals were euthanized, fixed and immunolabeled following the same protocol used for tree shrews.

Immunohistochemistry

Wholemount retinas were blocked for 1–3 hours in a PBS with 3% normal donkey serum, 0.3% Triton X-100, and 0.02% NaAzide. Pieces were then incubated in primary antibody solution at 4°C for 5–9 days. Following incubation in the primary antibody, retinas were washed with PBS 2–3 times over the course of 2 hours at room temperature. Retinas were then incubated in a secondary antibody overnight at 4°C. Following incubation in the secondary antibody, retinas were again washed with PBS 2–3 times over the course of 2 hours at room temperature. All incubations and washes were done on a mechanical rocker. Following antibody labeling, retinas were mounted onto filter paper (0.4UM type HABP, Millipore) to flatten the tissue. Retina and filter paper were then mounted together onto a glass slide with Aqua PolyMount or DiamondMount (Thermo Fisher Scientific). Glass coverslips were placed on either side of the filter paper and a third glass coverslip was placed over the filter paper and retina, resting on the adjacent coverslips to prevent over-flattening the retina. The coverslips were sealed with transparent nail polish.

Retinal slices were blocked for 30 minutes in a PBS with 3% normal donkey serum, 0.3% Triton X-100, and 0.02% NaAzide blocking buffer. Following block, slices were incubated in primary antibody solution at 4°C overnight. Following incubation in primary antibody, retinal slices were washed with PBS twice over 10 minutes at room temperature. Slices were then incubated in secondary antibody for two hours at room temperature. Following the secondary incubation, slices were washed again with PBS twice over 10 minutes at room temperature. Mounted slices were then immediately coverslipped in Aqua PolyMount. All incubations and washes were done in a humid chamber filled with deionized water.

The primary and secondary antibodies used in this study and their dilutions are listed in Tables 1 and 2, respectively. All primary and secondary antibodies were diluted in a PBS + 3% normal donkey serum + 0.3% Triton X-100 + 0.02% NaAzide blocking buffer. All secondary antibodies were obtained from donkey and were produced by Jackson ImmunoResearch Laboratories and diluted 1:1000. Hoechst (Thermo Fisher Scientific: H21491) was used as a nuclear stain to label all cell bodies (dilution: 1:1000). It was applied concurrently with secondary antibodies.

Imaging

Retinas were imaged on a Nikon TE 2000 Confocal Microscope C90i controlled by NIS-AR software (Nikon Instruments, RRID: SCR_014329). Images were processed using ImageJ (RRID: SCR_003070) or NIS-AR software.

Cell counting and ipRGC density analysis

Cell counting (Fig. 8) was performed using ImageJ (FIJI). Cells were manually counted using the cell counter tool (Analyze Plugin). The retina was cut into four separate pieces and cells were counted separately in each quadrant. Each identified ipRGC was assigned to a group: the first group of cells had somata in the ganglion cell layer (GCL) with sparse bistratified dendrites; the second group had somata in the inner nuclear layer (INL) and were immunoreactive for TH in addition to melanopsin; the third group had somata in the INL, but were negative for TH immunoreactivity; the fourth group had somata in the GCL that were weakly immunoreactive for melanopsin and monostratified dendrites that branched frequently. Cell location was marked by manually clicking the center of each cell body. The position and labeled type of each cell was exported to MATLAB (RRID: SCR_001622) for generating color maps of ipRGC density for each retinal quadrant. The quadrants were aligned and spaced using photographs of the dissected and immunolabeled retina to identify the position and orientation of each quadrant relative to the optic nerve head.

Cell reconstructions and stratification color map

Dendritic fields were reconstructed from z-stacks of confocal images (20× objective: 1 to 1.5 μm steps size). The Simple Neurite Tracer plugin for ImageJ was used to trace processes from the cell body (Longair, Baker, & Armstrong, 2011). After generating a skeleton of the dendritic arbor, the ‘fill tool’ in the plugin was used to reconstruct a 3D model of the cell. The threshold on the fill tool was adjusted manually to prevent over or under filling of the dendritic arbor. An image stack was created from the filled cell to generate an isolated 3D model of the cell and the Temporal Color Code tool under hyperstacks was used to map the Z (depth) axis to the ‘ice’ color map (Fig. 3). Z-stacks were cropped to constrain the color map between the GCL and the INL.

To analyze the spatial arrangement and overlap across dendritic fields (Fig. 7), en face images of individual cells were generated by hand drawing the images in software (Intaglio, Purgatory Design). Convex polygons (hulls) were then manually drawn around each cell. The coordinates of these polygons were exported to MATLAB. Polygons were mirrored about their center of mass using custom software written in MATLAB. Changes in spatial coverage after polygon rotation were measured by quantifying the area that was uncovered by any polygon in the original image and in the rotated polygon image.

Analysis of soma locations

The spatial organization of somata were analyzed by generating density recovery profiles (DRP; (Rodieck, 1991)) (Fig. 7). From the DRP analysis, an effective exclusion radius can be obtained as described in Rodieck (1991).

Results

Diverse cell types are melanopsin immunoreactive in tree shrew retina

To determine the density, diversity, and arrangement of ipRGCs in tree shrew, retinas were immunolabeled with antibodies against melanopsin (Hattar et al., 2002; Vuong, Hardi, Barnes, & Brecha, 2015; Karnas et al., 2013). The somas of melanopsin immunoreactive

(MEL+) cells were observed in the ganglion cell layer (GCL) and the inner nuclear layer (INL) (Fig. 1). The number of MEL+ cells in the INL was greater than in the GCL; 65% of MEL+ somata were in the INL (1981 of 2899 and 2136 of 3272 in two retinas). MEL+ cells in the GCL had two to three primary dendrites, while those in the INL typically exhibited four primary dendrites (Fig. 2A). Cells in the two layers also differed substantially in dendritic field area (Fig. 2B): cells in the GCL and INL had mean dendritic field areas of 0.05 ± 0.004 cm^2 and 0.019 ± 0.0014 cm^2, respectively. The dendrites of MEL+ somata in the GCL and INL ramified in specific sublayers of the inner plexiform layer (IPL). As described previously (Vaney, Peichi, & Boycott, 1981; Müller & Peichl, 1991b; Manookin, Beaudoin, Ernst, Flagel, & Demb, 2008; Hannibal, Christiansen, Heegaard, Fahrenkrug, & Kiilgaard, 2017), immunoreactivity for ChAT divided the IPL into 5 sublayers, labeled S1 to S5 from the INL to GCL. S2 and S4 were defined by the two bands of ChAT-positive immunoreactivity (Fig. 2C). MEL+ processes in the IPL were largely restricted to S1 and S5. These results reveal an organization of MEL+ cells and their processes that is broadly consistent with other mammals (Schmidt, Chen, & Hattar, 2011; Jusuf et al., 2007; Liao et al., 2016).

The observation of melanopsin-expressing cell somata in the GCL and INL with differences in their dendritic field areas and number of primary dendrites (Fig. 2A–B) suggests that multiple distinct cell types are intrinsically photosensitive. To further examine their morphological diversity, the dendritic fields of individual MEL+ cells were reconstructed from image stacks collected on a confocal microscope (Fig. 3). This analysis revealed several distinct morphologies. In the GCL, most MEL+ cells were bistratified. Their dendrites ramified in S1 and S5 of the IPL (Fig. 3A–C: S1 and S5 processes are red/purple and cyan/blue, respectively). Individual dendrites could course exclusively in S5, or they could run for some distance in S5 before branching or projecting to S1. The number of processes that remained in S5 versus projected to S1 varied across cells. These cells broadly resembled M1/M3 cells described previously in rodent and primate retinas (Hattar et al., 2002; Jusuf et al., 2007; Schmidt & Kofuji, 2009; Liao et al., 2016). However, because M1 in other species are monostratified in S1 (Schmidt et al., 2011) and M3 cells are bistratified but sparse (Berson, Castrucci, & Provencio, 2010; Nasir-Ahmad et al., 2017), we refer to these cells as bistratified ipRGCs (see Discussion).

A minority of MEL+ cells in the GCL exhibited a distinct morphology (Fig. 3D, 3%, 27 of 918 cells, and 7%, 81 of 1163, in two retinas). These cells were monostratified in S5 and exhibited relatively densely branching dendrites. Furthermore, these cells were weakly melanopsin immunoreactive relative to the bistratified cells (not shown). These cells resembled M2 cells described previously in rodent and primate retinae (Baver, Pickard, Sollars, & Pickard, 2008; Schmidt & Kofuji, 2009; Berson et al., 2010). We henceforth refer to these as monostratified inner ipRGCs because of the structure and stratification of their dendrites.

In the INL, the majority of MEL+ cells exhibited monostratified dendritic fields that stratified in S1 (Fig. 3E–F, 87%: 1868 of 2136 and 1725 of 1981 in two retinas). They typically exhibited four primary dendrites. These cells did not have a clear morphological

homologue in other previously studied mammals. Below, we show these cells were also immunolabeled for TH.

The remainder of MEL+ cells with somata in the INL (13%, 268 of 2136 and 256 of 1981 in two retinas) exhibited bistratified dendritic fields that were similar to the bistratified ipRGCs in the GCL (Fig. 3G); their dendritic fields were relatively sparse, and they typically exhibited two or three primary dendrites. For reasons described below, these cells are likely displaced bistratified ipRGCs.

To summarize, three dimensional reconstructions of MEL+ cells revealed at least three morphologically distinct classes that were distinguished based on their soma location, dendritic field structure, and stratification.

Cells co-immunolabeled for tyrosine hydroxylase and melanopsin

We next sought molecular markers that would bolster discriminating and classifying the different MEL+ cells. In rodents and primates, some ipRGCs exhibit a tight interaction with dopaminergic amacrine cells (DACs) (Vugler et al., 2007; Liao et al., 2016). In particular, these ipRGCs both receive and provide input to DACs (Zhang et al., 2008; Van Hook, Wong, & Berson, 2012; Prigge et al., 2016; Vuong et al., 2015; Liao et al., 2016). Thus, these interactions are a feature that may distinguish ipRGC subtypes.

Retinas were co-immunolabeled with antibodies against melanopsin and TH (Samaco et al., 2009); TH is a key enzyme in the synthesis of dopamine and is indicative of dopaminergic cells in the retina (Iuvone, Galli, Garrison-Gund, & Neff, 1978; Brecha, Oyster, & Takahashi, 1984; Nguyen-Legros, Botteri, Phuc, Vigny, & Gay, 1984; Müller & Peichl, 1991b). The somata of TH immunolabeled (TH+) cells in tree shrew retinas were limited to the inner boundary in the INL (Fig. 4A). They exhibited a network of dendritic processes restricted to S1 of the IPL (Fig. 2C). Surprisingly, all TH+ cells were also MEL+ (Fig. 4B–C, filled arrowheads). Some MEL+ cells with somata in the INL were TH negative (Fig. 4C, open arrowhead). These TH-negative cells were 13% of all MEL+ cells in the INL, the same fraction of cells that were bistratified with somata in the INL (Fig. 3G). Inspection of cells in the INL that did not label for TH revealed they were bistratified. Thus, immunoreactivity for TH confirmed the morphological observation of at least two distinct classes of MEL+ cells with somata in the INL.

In other mammals, antibodies to TH and MEL label distinct classes of neurons in the retina: amacrine cells and RGCs, respectively (Vugler et al., 2007; Dumitrescu, Pucci, Wong, & Berson, 2009; Prigge et al., 2016; Liao et al., 2016; Hannibal et al., 2017). Thus, the observation of a population of retinal cells that are MEL+ and TH+ is unusual and surprising. It suggests a set of cells that is both intrinsically photosensitive and dopaminergic. An alternative possibility is that there is cross reactivity between antibodies. TH antibodies could be binding melanopsin. This is unlikely because we observed cells in the INL and GCL that were MEL+ and TH-(Fig. 4C–D). We also tested a second TH antibody (Millipore: MAB318), and observed the same pattern of labeling, with negligible background labeling in the GCL (Fig. 4G–L). Another possibility is that the MEL antibodies are binding TH. To test this, we repeated these experiments in another species, the Nile rat

(Langel, Smale, Esquiva, & Hannibal, 2015). Like tree shrews, Nile rats are diurnal, and they have cone-enriched retinas (~35% of photoreceptors are cones (Gaillard et al., 2008; Gaillard, Kuny, & Sauvé, 2009)). In Nile rats, TH+ and MEL+ cells formed two distinct and non-overlapping cell populations, similar to other mammals (Fig. 5). This result argues against the melanopsin antibody used here binding TH. It also suggests that the apparent co-expression of TH and MEL in a single cell population may be unique to tree shrews; it is not a general feature of animals with cone-enriched retinas, though tree shrews have a much higher proportion of cones than Nile rats. We also performed these experiments in C57bl/6J mice. We observed two non-overlapping populations of TH+ or MEL+ cells (data not shown), consistent with previous studies (Dumitrescu et al., 2009). Thus, we view it unlikely that these results are caused by a lack of specificity in the antibodies.

Are tyrosine hydroxylase positive cells RGCs or amacrine cells?

The observation of putative coexpression of TH and MEL in a cell class raises the question of whether these cells are amacrine cells or RGCs. To distinguish these possibilities, we performed a series of immunolabeling experiments. In the first set of experiments, we tested for co-labeling of TH with several amacrine cell markers. DACs in rodents are also GABAergic, and antibodies to GABA or proteins involved in its production (e.g. GAD67) immunolabel these cells (Kosaka et al., 1987; Wässle & Chun, 1988; Wulle & Wagner, 1990; Contini & Raviola, 2003). Furthermore, these antibodies do not label RGCs. Thus, we tested for co-labeling of antibodies to GABA and GAD67 with TH. Neither of these amacrine cell markers exhibited co-labeling with TH (Fig. 6A–H), despite labeling at least some amacrine cells (Fig. 6G–H).

We next tested whether antibodies to activation protein AP-2α, which labels all amacrine cells in mice (Bisgrove & Godbout, 1999; Bassett et al., 2007), co-labeled TH positive cells in tree shrew. We first tested whether AP-2α robustly labels amacrine cells in tree shrew by comparing the pattern of labeling between AP-2α and RBPMS, a specific and ubiquitous marker of RGCs (Rodriguez et al., 2014). We found these two markers labeled non-overlapping populations of cells in the GCL (Fig. 6I–J). These experiments support the conclusion that AP-2α labels amacrine cells specifically and ubiquitously in tree shrew, as it does in mouse. However, AP-2α and TH immunoreactivity were never localized to the same cells in the INL (Fig. 6K–P). These experiments suggest that TH+ cells in tree shrew are not amacrine cells.

After testing amacrine specific markers, we turned to specific markers for RGCs to test whether they co-labeled TH+ and MEL+ cells. We again used RBPMS as a specific and ubiquitous marker for RGCs (Rodriguez et al., 2014). MEL+ cells in the GCL were RBPMS + (data not shown). TH+ positive cells in the INL also immunolabeled for RBPMS (Fig. 6P). In summary, the pattern of labeling produced by antibodies that distinguish amacrine cells from RGCs support the possibility that TH+/MEL+ cells are RGCs.

Immunolabeling with RBPMS also allowed us to approximate the fraction of RGCs that were intrinsically photosensitive. In a patch of peripheral tree shrew 0.2 mm^2, 1225 RBPMS positive and AP-2α negative somata were identified along with 9 MEL+ somata, all in the GCL. This indicates that at least ~0.7% of all RGCs are ipRGCs, or at least ~2.1% if TH

+/MEL+ cells are considered RGCs and included in this count. These numbers are lower bounds as we may not be identifying all M2-like cells (see Discussion).

Melanopsin positive cells form at least two independent mosaics

The immunolabeling and morphological analyses described above suggest three ipRGC types in tree shrew: bistratified ipRGCs (~23% of which are displaced), M2-like ipRGCs, and TH+/MEL+ cells. To further explore this hypothesis, we examined how these cells were distributed and organized across space. M2-like cells were too few to support this analysis (see Discussion), so only TH+/MEL+ and bistratified cell populations were examined.

A hallmark of retinal cell types is regularly spaced somata with dendritic fields that approximately tile space (Wassle & Riemann, 1978; Wassle, Peichl, & Boycott, 1981b; Wassle, Peichl, & Boycott, 1981b; Dacey, 1993; Gauthier et al., 2009; Field & Chichilnisky, 2007). To test for regular spacing among somata, we generated density recovery profiles (DRPs; Fig. 7A–D), which are radial spatial autocorrelation functions (Rodieck, 1991). Regularly spaced cells exhibit a spatial refractory period between neighbors. The DRPs for both TH+/MEL+ and bistratified cells indicated a dearth of neighbors at short distances (Fig. 7B & D). An effective exclusion radius was calculated from each DRP (Rodieck, 1991). TH +/MEL+ and bistratified cells had exclusion radii of 116 μm and 148 μm, respectively. These exclusion DRPs and exclusion radii were calculated from somata locations in the nasal-ventral quadrant of the retina, where cell density was relatively low and density gradients were relatively flat (see below). Thus, these exclusion radii will be smaller in areas of retina with higher densities of MEL+ cells. Nevertheless, this analysis indicates homotypic repulsion between neighboring cells, thus supporting the conclusion that these populations form irreducible cell types.

The second hallmark of retinal cell types is a tendency toward spatial coordination among dendritic fields to tile space (Wassle et al., 1981b; Wassle, 2004; Reese & Keeley, 2015). To test for this coordination, convex hulls were generated from the dendritic fields of TH+/MEL + and bistratified cells (Figs. 7E–F). The dendrites of TH+/MEL+ cells approximately tiled space, particularly avoiding gaps (Fig. 7E). To test whether the shapes of the dendritic fields were coordinated, each convex hull was rotated 180°, which revealed 6.62-fold increase in the area that went unsampled between neighboring cells (compare black area between Figs. 7G & H).

These analyses support the conclusion that the population of TH+/MEL+ cells exhibits coordination among dendritic fields to approximately tile space.

We performed the same analysis of dendritic field coordination for bistratified cells (Fig. 7F). Interestingly, dendritic field sampling among cells with somata in the GCL were largely filled by cells with somata in the INL (Fig. 7F, thinly vs. thickly outlined polygons). Rotating the convex hulls that outlined the dendritic fields by 180° also resulted in a 2.18-fold increase in gaps between neighboring bistratified ipRGC dendritic fields (Figs. 7I & J). These analyses support the conclusion that the population of bistratified ipRGCs exhibits coordination among dendritic fields to approximately tile space.

To summarize, these analyses indicate that the bistratified and TH+/MEL+ cells each exhibit regularly spaced somata and coordinated dendritic field coverage, two defining features of irreducible retinal cell types.

Melanopsin positive cells exhibit a peak in density near in the ventral-temporal retina

Distinct RGC types, including ipRGCs, can exhibit distinct spatial gradients across the retina (Peichl, 1989; Bleckert, Schwartz, Turner, Rieke, & Wong, 2014; Hughes, Watson, Foster, Peirson, & Hankins, 2013; Valiente-Soriano et al., 2014). Thus, we analyzed the spatial distribution of melanopsin immunolabeled cells across the tree shrew retina. Two retinas were analyzed: one right and one left retina from different animals. The two retinas (right and left) from two different animals contained 2899 and 3272 MEL+ cells, respectively (Fig. 8A–B). The 11% difference in cell counts is likely due to some peripheral retina being lost in the eye with fewer cells. MEL+ cells were not uniformly distributed. A clear peak in density was in the temporal retina, just below the horizontal meridian in both eyes (Fig. 8A–B, yellow). We next tested whether this spatial arrangement was common among the different cell types. TH+/MEL+ cells exhibited a distinct distribution from bistratified cells. The density of bistratified cells was sharply peaked at 50–55 cells/mm^2, with a median density of ~10 cells/mm^2 (Fig. 8C–D, colormap and arrowhead). In contrast, TH+/MEL+ cells were more uniformly distributed across the retina with a peak and median densities of 35–40 cells/mm^2, and 15–20 cell/mm^2, respectively (Fig. 8E–F, colormap and arrowhead). Thus, different populations of MEL+ cells in the tree shrew exhibit distinct spatial distributions, suggesting that they may play different roles in image-forming and non-image-forming functions.

Discussion

Studies of mammalian retinae reveal a canonical organization that is tuned by evolution to meet the demands of different niches. For example, the primate retina exhibits specializations for high acuity, while the rodent retina commits a much higher fraction of cells to signaling motion. We have examined the organization and diversity of intrinsically photosensitive cells in the tree shrew to explore species-specific specializations of this key signaling pathway. We find evidence for three types of intrinsically photosensitive cells, one of which is likely to be dopaminergic. At least two of these cell types tile the retina with their dendritic fields. Furthermore, they exhibited distinct density gradients across eccentricity, suggesting different functions. We compare these results to those in primate and rodent retinae to identify the organizational features that are common across species and those that are distinct. We also comment on the apparent convergence of dopaminergic signaling and intrinsic photosensitivity in tree shrew retina -- two retinal signaling networks that are cellularly distinct in other mammals studied thus far. Finally, we comment on the benefits of tree shrews for vision research.

Comparison of melanopsin expression patterns across species

In mice and rats, five different ipRGC types have been identified through a confluence of morphological, genetic, and functional studies (Hattar et al., 2002; Ecker et al., 2010; Schmidt et al., 2011; Hu, Hill, & Wong, 2013; Zhao et al., 2014; Reifler et al., 2015). They

are frequently referred to as M1–M5. These cell types differ in their morphology, level of melanopsin expression, degree of intrinsic photosensitivity, projection patterns to the brain, and the behaviors they subserve (Sand et al., 2012). M1 cells exhibit large and sparse dendritic fields that ramify in S1 of the IPL; they are robustly immunolabeled for melanopsin (Hattar et al., 2002; Dacey et al., 2005; Jusuf et al., 2007). M2 cells exhibit smaller and more densely branching dendritic fields that stratify in S5 (Baver et al., 2008). M3 cells are sparsely distributed across the retina and have bistratified dendrites in S1 and S5 (Berson et al., 2010; Schmidt & Kofuji, 2011). M4 and M5 cells have lower levels of melanopsin expression -- too low to be detected with direct immunolabeling approaches (Ecker et al., 2010; Sand et al., 2012). Instead, these cells were identified by using a mouse line that expresses Cre under the OPN4 promoter (Ecker et al., 2010): M4 cells are likely alpha-RGC, which project to the superior colliculus and dorsal lateral geniculate nucleus (Estevez et al., 2012; Schmidt et al., 2014). M5 cells are significantly smaller with ‘bushy’ dendritic fields (Ecker et al., 2010). This diversity illustrates that melanopsin-mediated signaling contributes to many of the parallel pathways that emanate from the rodent retina.

It is important to note that the diversity of ipRGCs in rodent remains to be fully resolved. Recent work suggests M1 cells may in fact be at least two cell types in mice. First, the organization of their dendrites exhibits a relatively high coverage factor and does not exhibit the orderly and regular spatial tiling typically observed among most other RGC types (Berson et al., 2010). Second, M1 cells can be subdivided based on their expression of Brn3b, which corresponds to differential roles for Brn3b negative cells in the pupillary light response and Brn3b positive cells in circadian entrainment (Chen, Badea, & Hattar, 2011; Jain, Ravindran, & Dhingra, 2012). Finally, the status of M3 cells as a genuinely distinct type is questionable; they are few in number across the mouse retina and they may merely represent variability in the morphology of M1 cells. Electrophysiology experiments in the rat retina also indicated M3 cells are less frequently encountered than the other four types (Reifler et al., 2015), further suggesting they may represent morphological variability among M1 cells.

An examination of nonhuman primate and human retinae produces a somewhat different picture. In primates, ipRGCs appear to be comprised of just two types, M1 and M2 cells (Dacey et al., 2005; Jusuf et al., 2007; Liao et al., 2016; Nasir-Ahmad et al., 2017; Hannibal et al., 2017). M1 and M2 cells have dendrites limited to S1 and S5, respectively, and each appears to tile the retina. M1 cells are immunolabeled more strongly for melanopsin than M2 cells, suggesting a higher expression level of the protein (Liao et al., 2016; Nasir-Ahmad et al., 2017). M3 cells have also been observed in primate (Nasir-Ahmad et al., 2017), though as with rodents, these cells are rare and may arise just from morphological variability in another ipRGC type. Unlike mice, the diversity and organization of ipRGCs in primate is currently limited to immunolabeling, which may result in a failure to identify RGCs with weaker expression levels of melanopsin, such as M4 and M5 cells in rodent. Nevertheless, studies in new world monkeys (marmosets), old world monkeys (macaques) and humans, provide a relatively consistent view of ipRGC diversity and organization. Functionally, ipRGCs in primates may serve somewhat different roles as well. For example, primate ipRGCs can exhibit cone-opponent responses (Dacey et al., 2005), a response property that has not been observed in the ipRGCs of rodents.

In tree shrew, we find an organization of melanopsin immunoreactive cells that has some similarities and differences with rodents and primates. Similar to these species, tree shrews exhibit at least two types of ipRGCs with dendrites stratifying in S1 and/or S5 of the IPL. The least numerous cells we observed, those that were monostratified in S5 (Fig. 3D), resemble M2 cells from primates and rodents. These cells did not show evidence of regular spacing or formation of a mosaic because we observed very few in any retina. Two issues may contribute to potentially undersampling M2 cells. First, M2 cells in other species exhibit weaker labeling and lower protein expression than M1 cells, making them somewhat more difficult to detect using immunohistochemical methods (Hattar et al., 2006; Schmidt & Kofuji, 2009). Second, the melanopsin antibody we used (PA1-781) is directed against the C-terminus of the protein and has been reported in rodents to label M1 cell preferentially (Baver et al., 2008). We tried an antibody directed against the N-terminus, which has been reported to label M2 cells (PA1-780), but we observed no labeling in tree shrew retina across a range of concentrations. Thus, future experiments are needed to resolve whether M2 cells in tree shrew tile the retinal like most RGC types (Field & Chichilnisky, 2007; Sanes & Masland, 2015), or sparsely sample the visual scene.

We also observed a set of bistratified ipRGCs, with dendrites ramifying in S1 and S5 of the IPL; ~23% of these cells exhibited somata in the INL, but their dendrites filled gaps in the dendritic coverage of cells with somata in the GCL, suggesting this is a single cell type. This is consistent with observations of displaced M1 cells in the primate retina filling gaps in dendritic coverage of M1 cells with somata in the GCL (Jusuf et al., 2007). Thus, this population is most similar to M1/M3 cells in rodents and primates: They are unlike M1 because they are typically bistratified, but they are unlike M3 cells because their dendrites tile space and their somata are regularly spaced.

The most numerous cell type that immunolabeled for melanopsin exhibits cell bodies in the INL, dendrites in S1, and co-immunolabeled for TH. This pattern of immunolabeling is surprising because it suggests that either tree shrews have an intrinsically photosensitive amacrine cell or a dopaminergic ipRGC. Given studies in other mammals, the location of their somata and their immunoreactivity to TH suggests they are amacrine cells. Indeed, a previous study in tree shrews examined TH+ cells and presumed they were amacrine cells (Müller & Peichl, 1991b). The cells they described are similar to the TH+ cell described here in every respect, so they are likely the same cells. However, in other mammals, DACs are immunopositive for GABA and enzymes involved in its synthesis, such as GAD67 (Kosaka et al., 1987; Wässle & Chun, 1988; Wulle & Wagner, 1990; Contini & Raviola, 2003). We did not find evidence for immunoreactivity for GABA, GAD67, or the pan-amacrine cell marker AP-2α (Fig. 6). The immunolabeling for melanopsin suggests these cells could be RGCs. We found these cells to co-label with RBPMS, an immunohistochemical marker for RGCs (Rodriguez et al., 2014). RGCs have been identified as residing in the INL in other vertebrates, such as fish (Cook & Becker, 1991; Cook, Kondrashev, & Podugolnikova, 1996). Typically, soma size is a feature that can assist in discriminating RGCs from amacrine cells: RGCs typically have larger somata. However, in many species DACs exhibit large somata that are ~15 μm in diameter, similar to the somata size we observed for these cells (Nguyen-Legros et al., 1984; Mariani, Kolb, & Nelson, 1984). Thus, our evidence is suggestive that TH+ cells may be RGCs, but is far from

conclusive. A recent study provided evidence for an intrinsically photosensitive interneuron in the extreme periphery of the mouse retina (Valiente-Soriano et al., 2014). Thus, a stronger test will be to identify axons that emerge from these cells and enter the optic nerve (Pang, Gao, & Wu, 2010; Valiente-Soriano et al., 2014). Axonal labeling by melanopsin antibodies in this study was generally weak and insufficient to clearly trace axons. Thus, future work to retrogradely label melanopsin immunoreactive cells will be required to fully resolve the identity of TH+/MEL+ cells.

We found that bistratified ipRGCs and TH+/MEL+ cells exhibited distinct spatial distributions across the retina. In primates, M1 and M2 cell densities peak in the region surrounding the fovea -- they are excluded from the fovea itself (Jusuf et al., 2007; Nasir-Ahmad et al., 2017). Tests for eccentricity-dependent density gradients among ipRGCs in mice have produced mixed results: a preponderance of evidence suggests a higher density in the superior than inferior retina (Hughes et al., 2013; Valiente-Soriano et al., 2014), and a higher density in temporal than nasal retina (Valiente-Soriano et al., 2014). The gradients were significantly different between M1 and M2 cells compared to M4 and M5, which ran in the opposite direction (Hughes et al., 2013). The distinct gradients of melanopsin immunolabeled cells that we observe in tree shrew supports the notion that they subserve distinct functions. In particular, bistratified ipRGCs may be participating in imaging forming or color vision because their density peaks at a location in each eye that corresponds to a binocular zone in front and slightly above the animal (Dacey et al., 2005; Johnson, Van Hooser, & Fitzpatrick, 2010). TH+/MEL+ cells were more uniformly distributed. A relatively uniform distribution may be beneficial for uniformly distributing dopamine, a paracrine neuromodulator, across the retina (Witkovsky, 2004).

Circadian and dopaminergic modulation

Animals must entrain their physiology to the behavioral demands imposed by night and day. Dopamine release and ipRGC signaling are two central components of this entrainment. For example, in the retina, dopamine release is high during day even in the absence of light (Pozdeyev & Lavrikova, 2000; Witkovsky, 2004). At night, melatonin release by photoreceptors is high and suppresses dopamine release (McMahon, Iuvone, & Tosini, 2014). This counterphase signaling likely tunes retinal signal processing for cone and rod-mediated vision. Thus, retinal signal processing is linked to the circadian rhythm. In rodents and primates, this link is at least partly formed by M1 ipRGCs, which provide intraretinal signaling to DACs. Specifically, they signal the ambient light level to DACs via axon collaterals that traverse the IPL (Zhang et al., 2008; Prigge et al., 2016; Joo, Peterson, Dacey, Hattar, & Chen, 2013). Furthermore, DACs provide dopaminergic and potentially GABAergic signals back onto ipRGCs (Van Hook et al., 2012; Contini & Raviola, 2003; Perez-Leon, Warren, Allen, Robinson, & Brown, 2006; Pack, Hill, & Wong, 2015). These likely reduce the gain of ipRGCs: The dopaminergic signals appear to act on ipRGCs through D1-like receptors to reduce their photocurrent and decrease their input resistance, thereby reducing intrinsic photosensitivity (Van Hook et al., 2012). Thus, ipRGCs drive DAC activity when stimulated by light, and DACs can modulate ipRGC gain in response to light, or in prediction of light -- in the case of circadian-driven release of dopamine.

Our results indicate that the organization of dopaminergic and melanopsin-mediated signaling in the tree shrew is distinct from other species. In particular, we find evidence that a single class of neurons is both dopaminergic and intrinsically photosensitive. Why would these systems converge in a single cell type in tree shrews? One possible explanation stems from the fact that tree shrews have very few rod photoreceptors compared to primates and rodents. Thus, this lack of rods opens the possibility that melanopsin-based photoreceptors may be the most sensitive photoreceptors in tree shrew. Indeed, the isomerization of a single melanopsin molecule can produce a substantial and sustained response in an ipRGC (Do et al., 2009). If dopamine release primes the retina for daylight conditions, it may be preferable to initiate dopamine release at luminances below the activation of cones. In this context, merging the dopaminergic system and melanopsin signaling into a single cell population has at least two advantages. First, at threshold, melanopsin-mediated signaling does not need to traverse a noisy synapse, making dopamine release less prone to synaptic noise from ipRGCs. Second, by expressing melanopsin, dopamine release could be driven by melanopsin-mediated depolarizations that are below spike threshold, making dopamine release more sensitive than if it required a presynaptic neuron to reach spike threshold. Thus, regardless of the identity of these cells (RGCs or amacrine cells), the convergence of melanopsin and dopamine signaling pathways in tree shrew may be a specialization to compensate for so few rod photoreceptors.

Tree shrews as a model for visual processing

Tree shrews have been used as a model system for central visual processing, particularly for understanding primary visual cortex. They exhibit specializations to early visual processing that are reminiscent of primates, such as a 6-layered lateral geniculate nucleus (Conway & Schiller, 1983; Conley et al., 1984; Holdefer & Norton, 1995), prominent color opponent neurons (Johnson et al., 2010), and a functional architecture in primary visual cortex (e.g. orientation columns) that is highly organized (Fitzpatrick, 1996; Van Hooser et al., 2013; Lee et al., 2016). However, relatively little is known about RGC diversity in the tree shrew, beyond ON and OFF and sustained vs. transient cells (van Dongen, ter Laak, Thijssen, & Vendrik, 1976). Recent work in the primate and rodent retinas suggest there are 30–40 distinct RGC types (Dacey, Peterson, Robinson, & Gamlin, 2003; Yamada, Bordt, & Marshak, 2005; Völgyi, Chheda, & Bloomfield, 2009; Sümbül et al., 2014; Baden et al., 2016; Sanes & Masland, 2015). This presents a challenge to fully understanding the processing that occurs from retina to cortex in these animals. It is clear their retinas are cone dominated (Müller & Peichl, 1989; Petry et al., 1993), and that they contain two types of horizontal cells (Müller & Peichl, 1993), starburst amacrine cells (Sandmann, Engelmann, & Peichl, 1997), rod bipolar cells (Müller & Peichl, 1991a), and at least a few functionally and morphologically distinct RGC types (van Dongen et al., 1976). We have added to the diversity of cell types in tree shrew with the addition of bistratified and M2-like ipRGCs. We have also added a third putative RGC type that is intrinsically photosensitive and potentially dopaminergic, though it remains possible this is an amacrine cell that is intrinsically photosensitive.

A complete accounting of RGC diversity in tree shrew has several potential benefits. One benefit is to understand evolutionary changes in retinal and visual system organization

between rodents and primates. For example, direction selective cells comprise ~20% of all RGCs in rodents, and probably only 1–3% in primates (Baden et al., 2016; Dacey, 2004). One potential reason for this difference is that primates devote a huge fraction (~55%) of their RGCs to ON and OFF midget cells to support high acuity vision (Dacey, 2004; Field & Chichilnisky, 2007). Determining whether tree shrews, which have 3–5-fold higher acuity than mice (Petry, Fox, & Casagrande, 1984; Prusky, West, & Douglas, 2000), exhibit a decrease in the proportion of direction selective RGCs and an increase in X-like or Y-like cells, may be a clue to when and where this trade-off initiated. It also remains unclear what determines and establishes the existence of orientation columns in primary visual cortex across species: mice do not have columns while primates do (Hubel & Wiesel, 1962; Ohki, Chung, Ch'ng, Kara, & Reid, 2005; Bonin, Histed, Yurgenson, & Reid, 2011; Ringach et al., 2016; Scholl, Pattadkal, Rowe, & Priebe, 2017; Scholl, Rylee, Luci, Priebe, & Padberg, 2017). The organization of the tree shrew retina, in comparison to that of mice and primates, may provide clues to the utility of orientation maps across species (Paik & Ringach, 2011; Hore, Troy, & Eglen, 2012). Furthermore, the genome of tree shrews has been sequenced recently (Fan et al., 2013), raising the possibility that a genomic comparison with mice and macaques may help to elucidate factors that control the relative production of distinct retinal cell types, and how these cells wire to various brain areas across different mammals.

Finally, tree shrews have been a highly productive model for studying myopia (Sherman, Norton, & Casagrande, 1977; Norton, 1990; Gawne, Siegwart, Ward, & Norton, 2017). Axial length of their eye changes in response to a variety of stimuli including stimulus blur and visual deprivation. A confluence of epidemiological and animal model studies implicates ambient light levels as a major contributor to the rise in myopia (Stone, Pardue, Iuvone, & Khurana, 2013; Norton & Siegwart, 2013). Specifically, indoor (photopic) lighting is typically 100–10,000-fold dimmer than outdoor (photopic) light, and children that spend more time outside have lower rates of myopia. Furthermore, increasing ambient lighting slows the effects of myopiagenic stimuli in animal models from chickens to tree shrews to nonhuman primates. It is also clear that dopamine signaling within the retina alters the progression rate of axial length changes and sensitivity to myopiagenic conditions. A key signaling pathway that can link high-lux environments to sustained dopamine release is the ipRGC system (Zhang et al., 2008; Prigge et al., 2016). Thus, understanding how dopaminergic and melanopsin signaling pathways interact in tree shrews may shed new insights into emmetropia and myopia.

Acknowledgments

We would like to thank A. Hall for assistance with cell tracing, V. Hoke and S. Frehling for assistance with harvesting eyes, H.M. Petry for discussions and providing some retinal tissue for early experiments, N. Anderson, S.D. Van Hooser and K.C. Hayes for providing Nile rat eyes, and T.C. Badea and M.T. Do for providing antibodies. The following funding agencies supported this work: Whitehead Scholars Award (G.D.F.), NEI R01-EY024567 (G.D.F.), Whitehall Foundation (G.D.F), the Max Planck Florida Institute for Neuroscience (D.F.), and the Core Grant for Vision Research to Duke University, EY005722.

References

Allen AE, Storchi R, Martial FP, Bedford RA, Lucas RJ. 2017; Melanopsin Contributions to the Representation of Images in the Early Visual System. Curr Biol. 27(11):1623–1632. [PubMed: 28528909]

Baden T, Berens P, Franke K, Román Rosón M, Bethge M, Euler T. 2016; The functional diversity of retinal ganglion cells in the mouse. Nature. 529(7586):345–350. [PubMed: 26735013]

Bassett EA, Pontoriero GF, Feng W, Marquardt T, Fini ME, Williams T, West-Mays JA. 2007; Conditional deletion of activating protein 2alpha (AP-2alpha) in the developing retina demonstrates non-cell-autonomous roles for AP-2alpha in optic cup development. Mol Cell Biol. 27(21):7497–7510. [PubMed: 17724084]

Baver SB, Pickard GE, Sollars PJ, Pickard GE. 2008; Two types of melanopsin retinal ganglion cell differentially innervate the hypothalamic suprachiasmatic nucleus and the olivary pretectal nucleus. Eur J Neurosci. 27(7):1763–1770. [PubMed: 18371076]

Berson DM, Castrucci AM, Provencio I. 2010; Morphology and mosaics of melanopsin-expressing retinal ganglion cell types in mice. J Comp Neurol. 518(13):2405–2422. [PubMed: 20503419]

Berson DM, Dunn FA, Takao M. 2002; Phototransduction by retinal ganglion cells that set the circadian clock. Science. 295(5557):1070–1073. [PubMed: 11834835]

Bisgrove DA, Godbout R. 1999; Differential expression of AP-2alpha and AP-2beta in the developing chick retina: repression of R-FABP promoter activity by AP-2. Dev Dyn. 214(3):195–206. [PubMed: 10090146]

Bleckert A, Schwartz GW, Turner MH, Rieke F, Wong RO. 2014; Visual space is represented by nonmatching topographies of distinct mouse retinal ganglion cell types. Curr Biol. 24(3):310–315. [PubMed: 24440397]

Bonin V, Histed MH, Yurgenson S, Reid RC. 2011; Local diversity and fine-scale organization of receptive fields in mouse visual cortex. J Neurosci. 31(50):18506–18521. [PubMed: 22171051]

Brecha NC, Oyster CW, Takahashi ES. 1984; Identification and characterization of tyrosine hydroxylase immunoreactive amacrine cells. Invest Ophthalmol Vis Sci. 25(1):66–70. [PubMed: 6142028]

Chen SK, Badea TH, Hattar S. 2011; Photoentrainment and pupillary light reflex are mediated by distinct populations of ipRGCs. Nature. 476(7358):92–5. [PubMed: 21765429]

Conley M, Fitzpatrick D, Diamond IT. 1984; The laminar organization of the lateral geniculate body and the striate cortex in the tree shrew (Tupaia glis). J Neurosci. 4(1):171–197. [PubMed: 6198492]

Contini M, Raviola E. 2003; GABAergic synapses made by a retinal dopaminergic neuron. Proc Natl Acad Sci U S A. 100(3):1358–1363. [PubMed: 12547914]

Conway JL, Schiller PH. 1983; Laminar organization of tree shrew dorsal lateral geniculate nucleus. J Neurophysiol. 50(6):1330–1342. [PubMed: 6663330]

Cook JE, Becker DL. 1991; Regular mosaics of large displaced and non-displaced ganglion cells in the retina of a cichlid fish. J Comp Neurol. 306(4):668–684. [PubMed: 2071699]

Cook JE, Kondrashev SL, Podugolnikova TA. 1996; Biplexiform ganglion cells, characterized by dendrites in both outer and inner plexiform layers, are regular, mosaic-forming elements of teleost fish retinae. Vis Neurosci. 13(3):517–528. [PubMed: 8782379]

Curcio CA, Sloan KRJ, Packer O, Hendrickson AE, Kalina RE. 1987; Distribution of cones in human and monkey retina: individual variability and radial asymmetry. Science. 236(4801):579–582. [PubMed: 3576186]

Dacey DM. 1993; The mosaic of midget ganglion cells in the human retina. J Neurosci. 13(12):5334–5355. [PubMed: 8254378]

Dacey, DM. Origins of perception: retinal ganglion cell diversity and the creation of parallel visual pathways. In: Gazzaniga, MS, editorThe Cognitive Neurosciences. Cambridge, MA: MIT Press; 2004. 281–301.

Dacey DM, Liao HW, Peterson BB, Robinson FR, Smith VC, Pokorny J, … Gamlin PD. 2005; Melanopsin-expressing ganglion cells in primate retina signal colour and irradiance and project to the LGN. Nature. 433(7027):749–754. [PubMed: 15716953]

Dacey DM, Peterson BB, Robinson FR, Gamlin PD. 2003; Fireworks in the primate retina: in vitro photodynamics reveals diverse LGN-projecting ganglion cell types. Neuron. 37(1):15–27. [PubMed: 12526769]

Do MT, Kang SH, Xue T, Zhong H, Liao HW, Bergles DE, Yau KW. 2009; Photon capture and signalling by melanopsin retinal ganglion cells. Nature. 457(7227):281–287. [PubMed: 19118382]

Dumitrescu ON, Pucci FG, Wong KY, Berson DM. 2009; Ectopic retinal ON bipolar cell synapses in the OFF inner plexiform layer: contacts with dopaminergic amacrine cells and melanopsin ganglion cells. J Comp Neurol. 517(2):226–244. [PubMed: 19731338]

Ecker JL, Dumitrescu ON, Wong KY, Alam NM, Chen SK, LeGates T, … Hattar S. 2010; Melanopsin-expressing retinal ganglion-cell photoreceptors: cellular diversity and role in pattern vision. Neuron. 67(1):49–60. [PubMed: 20624591]

Estevez ME, Fogerson PM, Ilardi MC, Borghuis BG, Chan E, Weng S, … Berson DM. 2012; Form and function of the M4 cell, an intrinsically photosensitive retinal ganglion cell type contributing to geniculocortical vision. J Neurosci. 32(39):13608–13620. [PubMed: 23015450]

Fan Y, Huang ZY, Cao CC, Chen CS, Chen YX, Fan DD, … Yao YG. 2013; Genome of the Chinese tree shrew. Nat Commun. 4:1426. [PubMed: 23385571]

Field GD, Chichilnisky EJ. 2007; Information processing in the primate retina: circuitry and coding. Annu Rev Neurosci. 30:1–30. [PubMed: 17335403]

Fitzpatrick D. 1996; The functional organization of local circuits in visual cortex: insights from the study of tree shrew striate cortex. Cereb Cortex. 6(3):329–341. [PubMed: 8670661]

Gaillard F, Bonfield S, Gilmour GS, Kuny S, Mema SC, Martin BT, … Sauvé Y. 2008; Retinal anatomy and visual performance in a diurnal cone-rich laboratory rodent, the Nile grass rat (Arvicanthis niloticus). J Comp Neurol. 510(5):525–538. [PubMed: 18680202]

Gaillard F, Kuny S, Sauvé Y. 2009; Topographic arrangement of S-cone photoreceptors in the retina of the diurnal Nile grass rat (Arvicanthis niloticus). Invest Ophthalmol Vis Sci. 50(11):5426–5434. [PubMed: 19553614]

Gauthier JL, Field GD, Sher A, Greschner M, Shlens J, Litke AM, Chichilnisky EJ. 2009; Receptive fields in primate retina are coordinated to sample visual space more uniformly. PLoS Biol. 7(4):e63.

Gawne TJ, Siegwart JT, Ward AH, Norton TT. 2017; The wavelength composition and temporal modulation of ambient lighting strongly affect refractive development in young tree shrews. Exp Eye Res. 155:75–84. [PubMed: 27979713]

Hannibal J, Christiansen AT, Heegaard S, Fahrenkrug J, Kiilgaard JF. 2017; Melanopsin expressing human retinal ganglion cells: Subtypes, distribution, and intraretinal connectivity. J Comp Neurol. 525(8):1934–1961. [PubMed: 28160289]

Hannibal J, Kankipati L, Strang CE, Peterson BB, Dacey D, Gamlin PD. 2014; Central projections of intrinsically photosensitive retinal ganglion cells in the macaque monkey. J Comp Neurol. 522(10): 2231–2248. [PubMed: 24752373]

Hattar S, Kumar M, Park A, Tong P, Tung J, Yau KW, Berson DM. 2006; Central projections of melanopsin-expressing retinal ganglion cells in the mouse. J Comp Neurol. 497(3):326–349. [PubMed: 16736474]

Hattar S, Liao HW, Takao M, Berson DM, Yau KW. 2002; Melanopsin-containing retinal ganglion cells: architecture, projections, and intrinsic photosensitivity. Science. 295(5557):1065–1070. [PubMed: 11834834]

Holdefer RN, Norton TT. 1995; Laminar organization of receptive field properties in the dorsal lateral geniculate nucleus of the tree shrew (Tupaiaglis belangeri). J Comp Neurol. 358(3):401–413. [PubMed: 7560294]

Hore VR, Troy JB, Eglen SJ. 2012; Parasol cell mosaics are unlikely to drive the formation of structured orientation maps in primary visual cortex. Vis Neurosci. 29(6):283–299. [PubMed: 23110776]

Hu C, Hill DD, Wong KY. 2013; Intrinsic physiological properties of the five types of mouse ganglion-cell photoreceptors. J Neurophysiol. 109(7):1876–1889. [PubMed: 23343892]

Hubel DH, Wiesel TN. 1962; Receptive fields, binocular interaction and functional architecture in the cat's visual cortex. J Physiol. 160:106–154. [PubMed: 14449617]

Hughes S, Watson TS, Foster RG, Peirson SN, Hankins MW. 2013; Nonuniform distribution and spectral tuning of photosensitive retinal ganglion cells of the mouse retina. Curr Biol. 23(17): 1696–1701. [PubMed: 23954426]

Iuvone PM, Galli CL, Garrison-Gund CK, Neff NH. 1978; Light stimulates tyrosine hydroxylase activity and dopamine synthesis in retinal amacrine neurons. Science. 202(4370):901–902. [PubMed: 30997]

Jain V, Ravindran E, Dhingra NK. 2012; Differential expression of Brn3 transcription factors in intrinsically photosensitive retinal ganglion cells in mouse. J Comp Neurol. 520(4):742–755. [PubMed: 21935940]

Johnson EN, Van Hooser SD, Fitzpatrick D. 2010; The representation of S-cone signals in primary visual cortex. J Neurosci. 30(31):10337–10350. [PubMed: 20685977]

Joo HR, Peterson BB, Dacey DM, Hattar S, Chen SK. 2013; Recurrent axon collaterals of intrinsically photosensitive retinal ganglion cells. Vis Neurosci. 30(4):175–182. [PubMed: 23834959]

Jusuf PR, Lee SC, Hannibal J, Grunert U. 2007; Characterization and synaptic connectivity of melanopsin-containing ganglion cells in the primate retina. Eur J Neurosci. 26(10):2906–2921. [PubMed: 18001286]

Kaas JH. 2008; The evolution of the complex sensory and motor systems of the human brain. Brain Res Bull. 75(2–4):384–390. [PubMed: 18331903]

Kaas JH. 2013; The Evolution of Brains from Early Mammals to Humans. Wiley Interdiscip Rev Cogn Sci. 4(1):33–45. [PubMed: 23529256]

Karnas D, Mordel J, Bonnet D, Pévet P, Hicks D, Meissl H. 2013; Heterogeneity of intrinsically photosensitive retinal ganglion cells in the mouse revealed by molecular phenotyping. J Comp Neurol. 521(4):912–932. [PubMed: 22886938]

Kosaka T, Kosaka K, Hataguchi Y, Nagatsu I, Wu JY, Ottersen OP, … Hama K. 1987; Catecholaminergic neurons containing GABA-like and/or glutamic acid decarboxylase-like immunoreactivities in various brain regions of the rat. Exp Brain Res. 66(1):191–210. [PubMed: 2884126]

Langel JL, Smale L, Esquiva G, Hannibal J. 2015; Central melanopsin projections in the diurnal rodent, Arvicanthis niloticus. Front Neuroanat. 9:93. [PubMed: 26236201]

Lazzerini Ospri L, Prusky G, Hattar S. 2017; Mood, the Circadian System, and Melanopsin Retinal Ganglion Cells. Annu Rev Neurosci. 40:539–556. [PubMed: 28525301]

Lee KS, Huang X, Fitzpatrick D. 2016; Topology of ON and OFF inputs in visual cortex enables an invariant columnar architecture. Nature. 533(7601):90–94. [PubMed: 27120162]

Li Q, Ni X. 2016; An early Oligocene fossil demonstrates treeshrews are slowly evolving “living fossils”. Sci Rep. 6:18627. [PubMed: 26766238]

Liao HW, Ren X, Peterson BB, Marshak DW, Yau KW, Gamlin PD, Dacey DM. 2016; Melanopsin-expressing ganglion cells on macaque and human retinas form two morphologically distinct populations. J Comp Neurol. 524(14):2845–2872. [PubMed: 26972791]

Lin J, Chen G, Gu L, Shen Y, Zheng M, Zheng W, … Jiang C. 2014; Phylogenetic affinity of tree shrews to Glires is attributed to fast evolution rate. Mol Phylogenet Evol. 71:193–200. [PubMed: 24333622]

Longair MH, Baker DA, Armstrong JD. 2011; Simple Neurite Tracer: open source software for reconstruction, visualization and analysis of neuronal processes. Bioinformatics. 27(17):2453–2454. [PubMed: 21727141]

Lucas RJ, Hattar S, Takao M, Berson DM, Foster RG, Yau KW. 2003; Diminished pupillary light reflex at high irradiances in melanopsin-knockout mice. Science. 299(5604):245–247. [PubMed: 12522249]

Manookin MB, Beaudoin DL, Ernst ZR, Flagel LJ, Demb JB. 2008; Disinhibition combines with excitation to extend the operating range of the OFF visual pathway in daylight. J Neurosci. 28(16): 4136–4150. [PubMed: 18417693]

Mariani AP, Kolb H, Nelson R. 1984; Dopamine-containing amacrine cells of rhesus monkey retina parallel rods in spatial distribution. Brain Res. 322(1):1–7. [PubMed: 6518360]

McMahon DG, Iuvone PM, Tosini G. 2014; Circadian organization of the mammalian retina: from gene regulation to physiology and diseases. Prog Retin Eye Res. 39:58–76. [PubMed: 24333669]

Morin LP, Blanchard JH, Provencio I. 2003; Retinal ganglion cell projections to the hamster suprachiasmatic nucleus, intergeniculate leaflet, and visual midbrain: bifurcation and melanopsin immunoreactivity. J Comp Neurol. 465(3):401–416. [PubMed: 12966564]

Müller B, Peichl L. 1989; Topography of cones and rods in the tree shrew retina. J Comp Neurol. 282(4):581–594. [PubMed: 2723153]

Müller B, Peichl L. 1991a; Rod bipolar cells in the cone-dominated retina of the tree shrew Tupaia belangeri. Vis Neurosci. 6:629–639. [PubMed: 1883767]

Müller B, Peichl L. 1991b; Morphology and distribution of catecholaminergic amacrine cells in the cone-dominated tree shrew retina. J Comp Neurol. 308(1):91–102. [PubMed: 1678751]

Müller B, Peichl L. 1993; Horizontal cells in the cone-dominated tree shrew retina: morphology, photoreceptor contacts, and topographical distribution. J Neurosci. 13(8):3628–3646. [PubMed: 7688042]

Müller B, Peichl L, De Grip WJ, Gery I, Korf HW. 1989; Opsin- and S-antigen-like immunoreactions in photoreceptors of the tree shrew retina. Invest Ophthalmol Vis Sci. 30(3):530–535. [PubMed: 2466810]

Nasir-Ahmad S, Lee SC, Martin PR, Grünert U. 2017Melanopsin-expressing ganglion cells in human retina: Morphology, distribution, and synaptic connections. J Comp Neurol. :1–16.

Nguyen-Legros J, Botteri C, Phuc LH, Vigny A, Gay M. 1984; Morphology of primate's dopaminergic amacrine cells as revealed by TH-like immunoreactivity on retinal flat-mounts. Brain Res. 295(1): 145–153. [PubMed: 6143588]

Nie W, Fu B, O'Brien PC, Wang J, Su W, Tanomtong A, … Yang F. 2008; Flying lemurs--the 'flying tree shrews'? Molecular cytogenetic evidence for a Scandentia-Dermoptera sister clade. BMC Biol. 6:18. [PubMed: 18452598]

Norton TT. 1990; Experimental myopia in tree shrews. Ciba Found Symp. 155:178–94. [PubMed: 2088676]

Norton TT, Siegwart JT. 2013; Light levels, refractive development, and myopia--a speculative review. Exp Eye Res. 114:48–57. [PubMed: 23680160]

Ohki K, Chung S, Ch'ng YH, Kara P, Reid RC. 2005; Functional imaging with cellular resolution reveals precise micro-architecture in visual cortex. Nature. 433(7026):597–603. [PubMed: 15660108]

Pack W, Hill DD, Wong KY. 2015; Melatonin modulates M4-type ganglion-cell photoreceptors. Neuroscience. 303:178–188. [PubMed: 26141846]

Packer O, Hendrickson AE, Curcio CA. 1989; Photoreceptor topography of the retina in the adult pigtail macaque (Macaca nemestrina). J Comp Neurol. 288(1):165–183. [PubMed: 2794135]

Paik SB, Ringach DL. 2011; Retinal origin of orientation maps in visual cortex. Nat Neurosci. 14(7): 919–925. [PubMed: 21623365]

Pang JJ, Gao F, Wu SM. 2010; Light responses and morphology of bNOS-immunoreactive neurons in the mouse retina. J Comp Neurol. 518(13):2456–2474. [PubMed: 20503422]

Peichl L. 1989; Alpha and delta ganglion cells in the rat retina. J Comp Neurol. 286(1):120–139. [PubMed: 2768556]

Perez-Leon JA, Warren EJ, Allen CN, Robinson DW, Brown RL. 2006; Synaptic inputs to retinal ganglion cells that set the circadian clock. Eur J Neurosci. 24(4):1117–1123. [PubMed: 16930437]

Petry HM, Erichsen JT, Szél A. 1993; Immunocytochemical identification of photoreceptor populations in the tree shrew retina. Brain Res. 616(1–2):344–350. [PubMed: 8358626]

Petry HM, Fox R, Casagrande VA. 1984; Spatial contrast sensitivity of the tree shrew. Vision Res. 24(9):1037–1042. [PubMed: 6506467]

Pozdeyev NV, Lavrikova EV. 2000; Diurnal changes of tyrosine, dopamine, and dopamine metabolites content in the retina of rats maintained at different lighting conditions. J Mol Neurosci. 15(1):1–9. [PubMed: 11211232]

Prigge CL, Yeh PT, Liou NF, Lee CC, You SF, Liu LL, … Zhang DQ. 2016; M1 ipRGCs Influence Visual Function through Retrograde Signaling in the Retina. J Neurosci. 36(27):7184–7197. [PubMed: 27383593]

Prusky GT, West PW, Douglas RM. 2000; Behavioral assessment of visual acuity in mice and rats. Vision Res. 40(16):2201–2209. [PubMed: 10878281]

Reese BE, Keeley PW. 2015; Design principles and developmental mechanisms underlying retinal mosaics. Biol Rev Camb Philos Soc. 90(3):854–876. [PubMed: 25109780]

Reifler AN, Chervenak AP, Dolikian ME, Benenati BA, Meyers BS, Demertzis ZD, … Wong KY. 2015; The rat retina has five types of ganglion-cell photoreceptors. Exp Eye Res. 130:17–28. [PubMed: 25450063]

Ringach DL, Mineault PJ, Tring E, Olivas ND, Garcia-Junco-Clemente P, Trachtenberg JT. 2016; Spatial clustering of tuning in mouse primary visual cortex. Nat Commun. 7:12270. [PubMed: 27481398]

Rodieck RW. 1991; The density recovery profile: a method for the analysis of points in the plane applicable to retinal studies. Vis Neurosci. 6(2):95–111. [PubMed: 2049333]

Rodriguez AR, de Sevilla Müller LP, Brecha NC. 2014; The RNA binding protein RBPMS is a selective marker of ganglion cells in the mammalian retina. J Comp Neurol. 522(6):1411–1443. [PubMed: 24318667]

Samaco RC, Mandel-Brehm C, Chao HT, Ward CS, Fyffe-Maricich SL, Ren J, … Neul JL. 2009; Loss of MeCP2 in aminergic neurons causes cell-autonomous defects in neurotransmitter synthesis and specific behavioral abnormalities. Proc Natl Acad Sci U S A. 106(51):21966–21971. [PubMed: 20007372]

Sand A, Schmidt TM, Kofuji P. 2012; Diverse types of ganglion cell photoreceptors in the mammalian retina. Prog Retin Eye Res. 31(4):287–302. [PubMed: 22480975]

Sandmann D, Engelmann R, Peichl L. 1997; Starburst cholinergic amacrine cells in the tree shrew retina. J Comp Neurol. 389(1):161–176. [PubMed: 9390767]

Sanes JR, Masland RH. 2015; The types of retinal ganglion cells: current status and implications for neuronal classification. Annu Rev Neurosci. 38:221–246. [PubMed: 25897874]

Schmidt TM, Alam NM, Chen S, Kofuji P, Li W, Prusky GT, Hattar S. 2014; A role for melanopsin in alpha retinal ganglion cells and contrast detection. Neuron. 82(4):781–788. [PubMed: 24853938]

Schmidt TM, Chen SK, Hattar S. 2011; Intrinsically photosensitive retinal ganglion cells: many subtypes, diverse functions. Trends Neurosci. 34(11):572–580. [PubMed: 21816493]

Schmidt TM, Do MT, Dacey D, Lucas R, Hattar S, Matynia A. 2011; Melanopsin-positive intrinsically photosensitive retinal ganglion cells: from form to function. J Neurosci. 31(45):16094–16101. [PubMed: 22072661]

Schmidt TM, Kofuji P. 2009; Functional and morphological differences among intrinsically photosensitive retinal ganglion cells. J Neurosci. 29(2):476–482. [PubMed: 19144848]

Schmidt TM, Kofuji P. 2011; Structure and function of bistratified intrinsically photosensitive retinal ganglion cells in the mouse. J Comp Neurol. 519(8):1492–1504. [PubMed: 21452206]

Schmitz J, Ohme M, Zischler H. 2000; The complete mitochondrial genome of Tupaia belangeri and the phylogenetic affiliation of scandentia to other eutherian orders. Mol Biol Evol. 17(9):1334–1343. [PubMed: 10958850]

Scholl B, Pattadkal JJ, Rowe A, Priebe NJ. 2017; Functional characterization and spatial clustering of visual cortical neurons in the predatory grasshopper mouse Onychomys arenicola. J Neurophysiol. 117(3):910–918. [PubMed: 27927787]

Scholl B, Rylee J, Luci JJ, Priebe NJ, Padberg J. 2017; Orientation selectivity in the visual cortex of the nine-banded armadillo. J Neurophysiol. 117(3):1395–1406. [PubMed: 28053246]

Sherman SM, Norton TT, Casagrande VA. 1977; Myopia in the lid-sutured tree shrew (Tupaia glis). Brain Res. 124(1):154–157. [PubMed: 843938]

Sonoda T, Schmidt TM. 2016; Re-evaluating the Role of Intrinsically Photosensitive Retinal Ganglion Cells: New Roles in Image-Forming Functions. Integr Comp Biol. 56(5):834–841. [PubMed: 27371393]

Spitschan M, Jain S, Brainard DH, Aguirre GK. 2014; Opponent melanopsin and Scone signals in the human pupillary light response. Proc Natl Acad Sci U S A. 111(43):15568–15572. [PubMed: 25313040]

Stone RA, Pardue MT, Iuvone PM, Khurana TS. 2013; Pharmacology of myopia and potential role for intrinsic retinal circadian rhythms. Exp Eye Res. 114:35–47. [PubMed: 23313151]

Sümbül U, Song S, McCulloch K, Becker M, Lin B, Sanes JR, … Seung HS. 2014; A genetic and computational approach to structurally classify neuronal types. Nat Commun. 5:3512. [PubMed: 24662602]

Szel A, Rohlich P, Caffe AR, Juliusson B, Aguirre G, Van Veen T. 1992; Unique topographic separation of two spectral classes of cones in the mouse retina. J Comp Neurol. 325(3):327–342. [PubMed: 1447405]

Szél A, Röhlich P, Caffé AR, van Veen T. 1996; Distribution of cone photoreceptors in the mammalian retina. Microsc Res Tech. 35(6):445–462. [PubMed: 9016448]

Valiente-Soriano FJ, García-Ayuso D, Ortín-Martínez A, Jiménez-López M, Galindo-Romero C, Villegas-Pérez MP, … Vidal-Sanz M. 2014; Distribution of melanopsin positive neurons in pigmented and albino mice: evidence for melanopsin interneurons in the mouse retina. Front Neuroanat. 8:131. [PubMed: 25477787]

van Dongen PA, ter Laak HJ, Thijssen JM, Vendrik AJ. 1976; Functional classification of cells in the optic tract of a tree shrew (Tupaia chinensis). Exp Brain Res. 24(4):441–446. [PubMed: 816664]

Van Hook MJ, Wong KY, Berson DM. 2012; Dopaminergic modulation of ganglion-cell photoreceptors in rat. Eur J Neurosci. 35(4):507–518. [PubMed: 22304466]

Van Hooser SD, Roy A, Rhodes HJ, Culp JH, Fitzpatrick D. 2013; Transformation of receptive field properties from lateral geniculate nucleus to superficial V1 in the tree shrew. J Neurosci. 33(28): 11494–11505. [PubMed: 23843520]

Vaney DI, Peichi L, Boycott BB. 1981; Matching populations of amacrine cells in the inner nuclear and ganglion cell layers of the rabbit retina. J Comp Neurol. 199(3):373–391. [PubMed: 6114966]

Viney TJ, Balint K, Hillier D, Siegert S, Boldogkoi Z, Enquist LW, … Roska B. 2007; Local retinal circuits of melanopsin-containing ganglion cells identified by transsynaptic viral tracing. Curr Biol. 17(11):981–988. [PubMed: 17524644]

Völgyi B, Chheda S, Bloomfield SA. 2009; Tracer coupling patterns of the ganglion cell subtypes in the mouse retina. J Comp Neurol. 512(5):664–687. [PubMed: 19051243]

Vugler AA, Redgrave P, Semo M, Lawrence J, Greenwood J, Coffey PJ. 2007; Dopamine neurones form a discrete plexus with melanopsin cells in normal and degenerating retina. Exp Neurol. 205(1):26–35. [PubMed: 17362933]

Vuong HE, Hardi CN, Barnes S, Brecha NC. 2015; Parallel Inhibition of Dopamine Amacrine Cells and Intrinsically Photosensitive Retinal Ganglion Cells in a Non-Image-Forming Visual Circuit of the Mouse Retina. J Neurosci. 35(48):15955–15970. [PubMed: 26631476]

Waddell PJ, Kishino H, Ota R. 2001; A phylogenetic foundation for comparative mammalian genomics. Genome Inform. 12:141–154. [PubMed: 11791233]

Wassle H. 2004; Parallel processing in the mammalian retina. Nat Rev Neurosci. 5(10):747–757. [PubMed: 15378035]

Wässle H, Chun MH. 1988; Dopaminergic and indoleamine-accumulating amacrine cells express GABA-like immunoreactivity in the cat retina. J Neurosci. 8(9):3383–3394. [PubMed: 2902202]

Wassle H, Peichl L, Boycott BB. 1981b; Dendritic territories of cat retinal ganglion cells. Nature. 292(5821):344–345. [PubMed: 7254331]

Wassle H, Peichl L, Boycott BB. 1981b; Morphology and topography of on- and off-alpha cells in the cat retina. Proc R Soc Lond B Biol Sci. 212(1187):157–175. [PubMed: 6166012]

Wassle H, Riemann HJ. 1978; The mosaic of nerve cells in the mammalian retina. Proc R Soc Lond B Biol Sci. 200(1141):441–461. [PubMed: 26058]

Witkovsky P. 2004; Dopamine and retinal function. Doc Ophthalmol. 108(1):17–40. [PubMed: 15104164]

Wulle I, Wagner HJ. 1990; GABA and tyrosine hydroxylase immunocytochemistry reveal different patterns of colocalization in retinal neurons of various vertebrates. J Comp Neurol. 296(1):173–178. [PubMed: 1972711]

Yamada ES, Bordt AS, Marshak DW. 2005; Wide-field ganglion cells in macaque retinas. Vis Neurosci. 22(4):383–393. [PubMed: 16212697]

Zhang DQ, Wong KY, Sollars PJ, Berson DM, Pickard GE, McMahon DG. 2008; Intraretinal signaling by ganglion cell photoreceptors to dopaminergic amacrine neurons. Proc Natl Acad Sci U S A. 105(37):14181–14186. [PubMed: 18779590]

Zhao X, Stafford BK, Godin AL, King WM, Wong KY. 2014; Photoresponse diversity among the five types of intrinsically photosensitive retinal ganglion cells. J Physiol. 592(7):1619–1636. [PubMed: 24396062]

Zhou X, Sun F, Xu S, Yang G, Li M. 2015; The position of tree shrews in the mammalian tree: Comparing multi-gene analyses with phylogenomic results leaves monophyly of Euarchonta doubtful. Integr Zool. 10(2):186–198. [PubMed: 25311886]

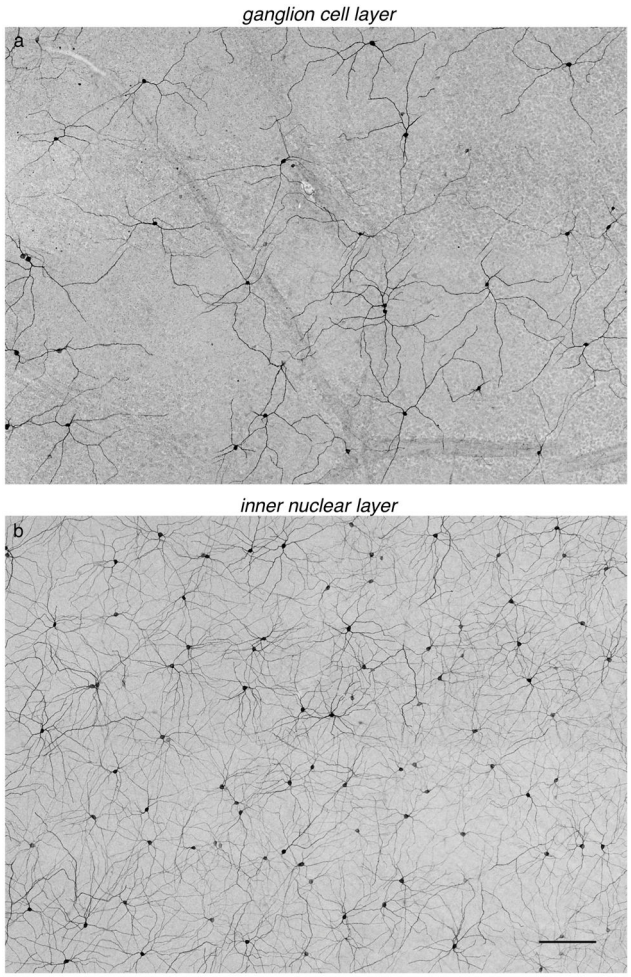

Figure 1.

Neurons in the GCL and INL are immunolabeled for melanopsin. (a) Image with focus set on the GCL showing neurons immunolabeled for melanopsin. (b) Same location in the retina as (a), but focused in the INL, shows cells immunolabeled for melanopsin. Scale bar: 200 μm.

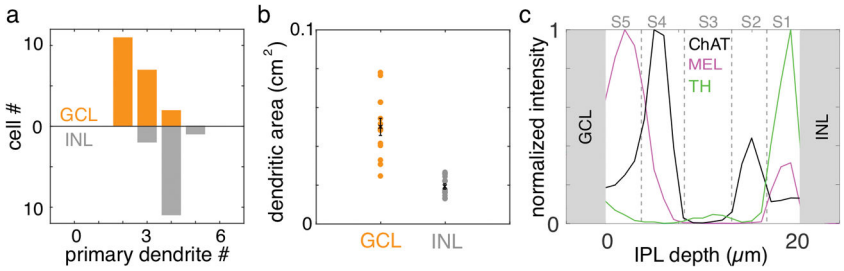

Figure 2.

Populations of MEL+ cells in the GCL and INL exhibit distinct dendritic field structures. (a) Distributions of primary dendrite number for MEL+ cells in the GCL and INL. (b) Dendritic field areas for MEL+ cells in the in the GCL and INL. (c) Normalized fluorescence intensity for immunolabeling of process in the IPL for melanopsin, ChAT and TH. ChAT immunolabeling is used to define sublayer S2 and S4 in the INL (top). MEL+ processes in the INL are largely restricted to S1 and S5.

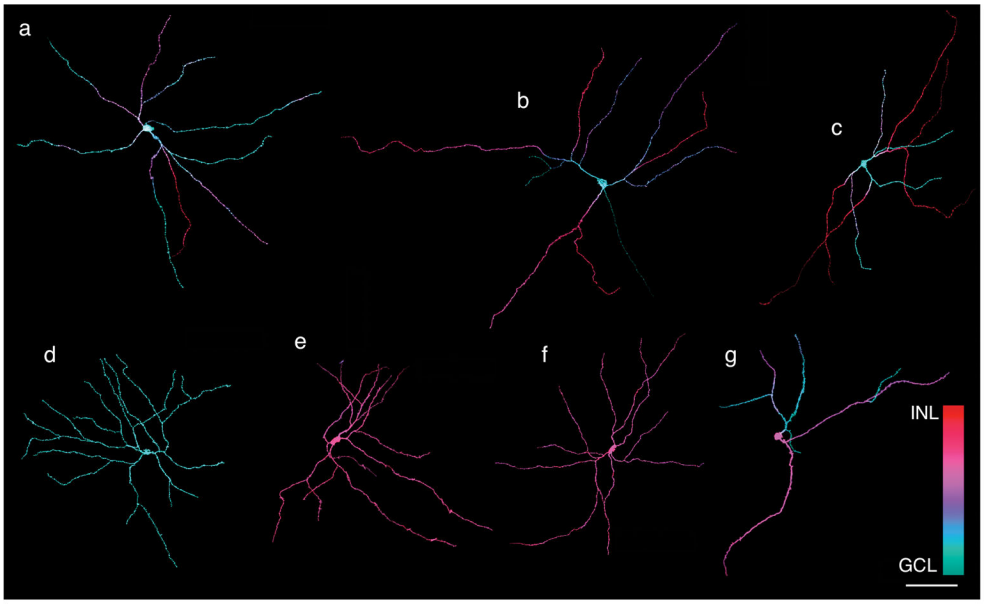

Figure 3.

Three-dimensional reconstructions of MEL+ neurons reveal several distinct morphologies. (a–c) Examples of bistratified RGC with somata in the GCL. Each cell is bistratified, but the number of dendrites in S1 (purple/red) and S5 (cyan/blue) varies across cells. (d) Example of an M2-like cell: soma is in the GCL, dendrites are restricted to S5. (e–f) Examples of MEL+ cells in with somata in the INL: dendrites are restricted to S1. (g) Example of a MEL + cell with soma in the INL and bistratified dendrites ramifying in S1 and S5. Scale bar: 100 μm.

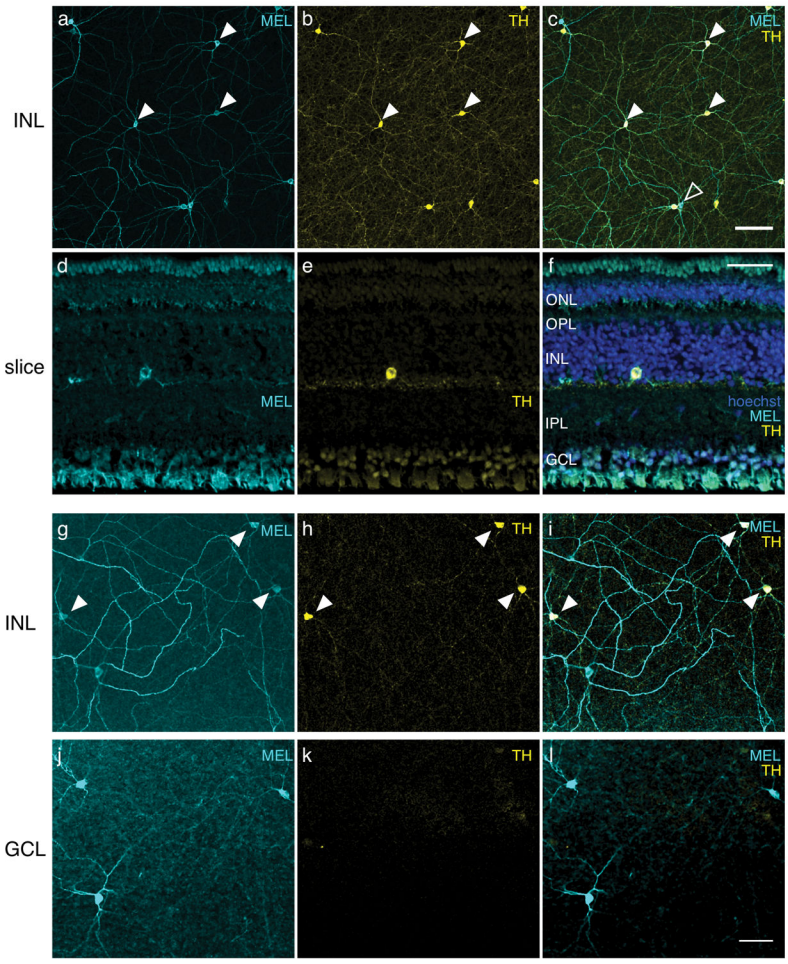

Figure 4.

Most cells immunoreactive to melanopsin (MEL) in the INL also exhibit immunoreactivity for TH. (a) MEL immunoreactivity in the INL. (b) TH immunoreactivity in the INL, same field of view as in (a). (c) Merge of (a) and (b). Eight of ten cells in the field of view were immunoreactive to anti-MEL and anti-TH; two of ten cells were immunoreactive to anti-MEL only. Closed arrowheads point to a subset of cells that are MEL and TH positive. Open arrowhead points to a cell that is only MEL+. No cells were TH+ and not MEL+. Scale bar: 100 μm. (d) Anti-MEL immunoreactivity in a transverse section. (e) Anti-TH immunoreactivity, field of view same as (d). (f) Merge of (d) and (e) with hoechst labeling. ONL, outer nuclear layer; OPL, outer plexiform layer; INL, inner nuclear layer; IPL, inner plexiform layer; GCL, ganglion cell layer. Scale bar: 50 μm. (g) MEL immunoreactivity in INL of a different retina. (h) TH immunoreactivity in the INL, same field of view as (g), but with a different TH antibody than that used in (a–f). I. Merge of (g) and (h). (j) Same field of view as (g), but focused on the GCL, showing MEL immunoreactivity. (k) Same field of view and focal plane as (j) showing TH immunoreactivity. (l) Merge of (j) and (k): Scale bar, 50 μm.

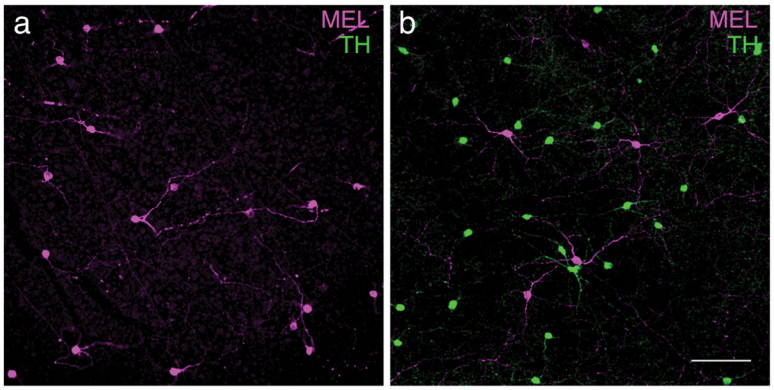

Figure 5.

Expression of MEL and TH is typical in Nile rat retina. (a) Anti-melanopsin and antiTH immunoreactivity in the GCL. Note, there was no TH immunoreactivity in the GCL. (b) Anti-melanopsin and anti-TH immunoreactivity in the INL, same retinal location as (a). Note that in the INL, TH+ cells are distinct from MEL+ cells. Scale bar: 100 μm.

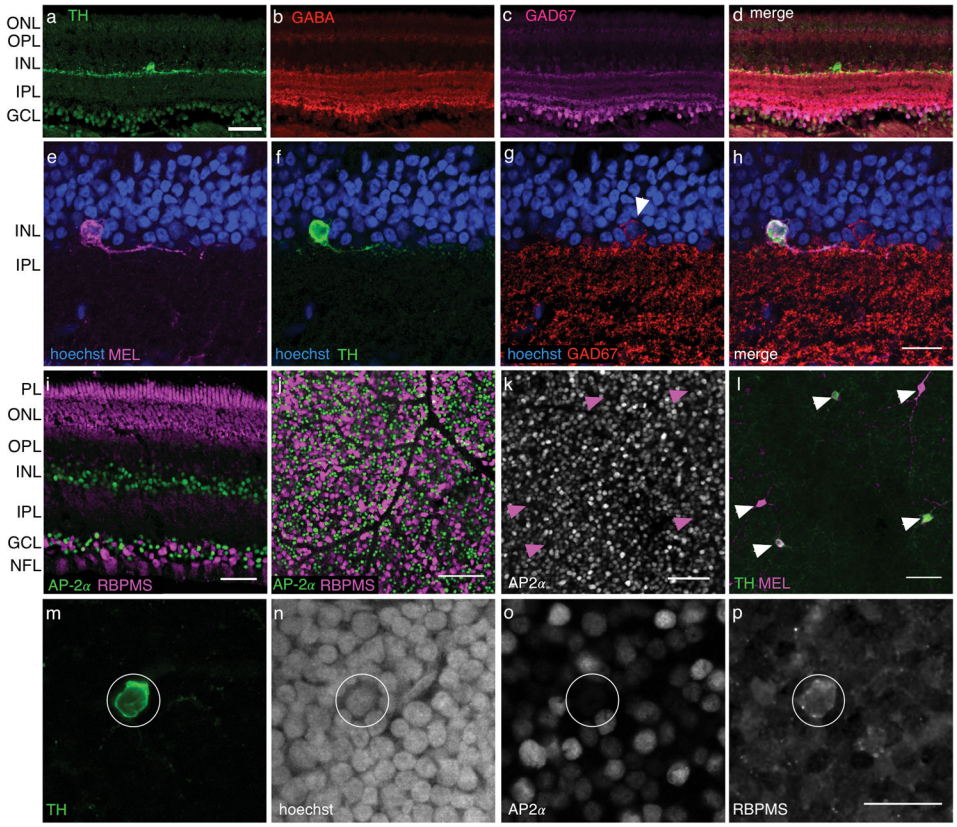

Figure 6.

TH+ cells immunolabel for RGC marker and not amacrine markers. (a) TH+ positive cell in cross section. Scale bar: 50 μm. (b–d) Same field of view as (a), but showing immunolabeling for GABA, GAD67 and a merge of all three channels, respectively. (e–h) MEL+ cell (e) that is also TH+ (f), but GAD67 negative (g), and a merge of all three labels with hoechst (h). Arrowhead in (g) indicates neighboring GAD67+ cell. Scale bar, 20 μm. (i) Comparison of labeling patterns for amacrine cell marker AP-2α and RBPMS in a transverse retinal slice. Scale bar: 50 μm. **J.** Comparison of labeling patterns for amacrine cell marker AP-2α and RBPMS in retinal whole mount, focused on the GCL. Scale bar: 100 μm. (k–l) AP-2α and TH labeling of the INL, respectively. Arrowheads indicate locations of TH+ cells in both images. (m–p) Example cell TH+ cell (m), showing hoechst labeling (n), and immunoreactivity for AP-2α (o) and RBPMS (p). Scale bar: 20 μm.

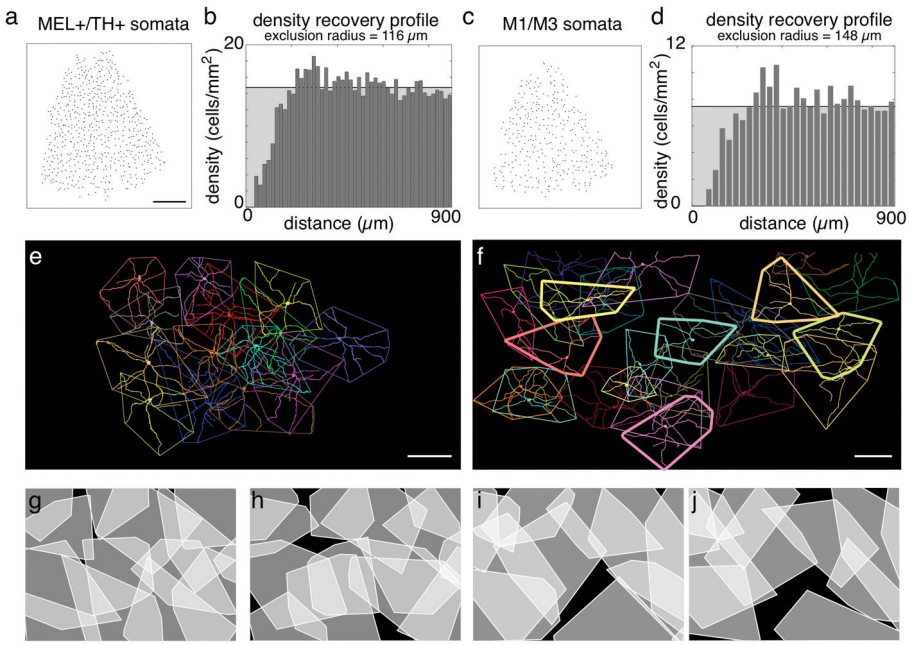

Figure 7.

TH+/MEL+ and bistratified cells form two distinct and irreducible cell types. (a) Locations of TH+/MEL+ somata in the INL of a nasal-ventral quadrant of retina. Scale bar: 1mm. (b) DRP for the soma locations in (a). Horizontal black line shows mean density. Randomly distributed points will form a flat DRP at the location of the black line. (c) Same as (b), for bistratified somata (in GCL and INL). (d) Same as (b), for locations in (c). (e) En face dendritic fields and convex hulls of a locally complete population of TH+/MEL+ cells. Scale bar: 200 μm. (f) Same and (e)., for bistratified cells. Scale bar: 200 μm. (g–h) Convex hulls for locally complete population of TH+/MEL+ cells (g) and same group but with hulls each rotated by 180°. (i–k) Same as (g–h), but for bistratified cells.

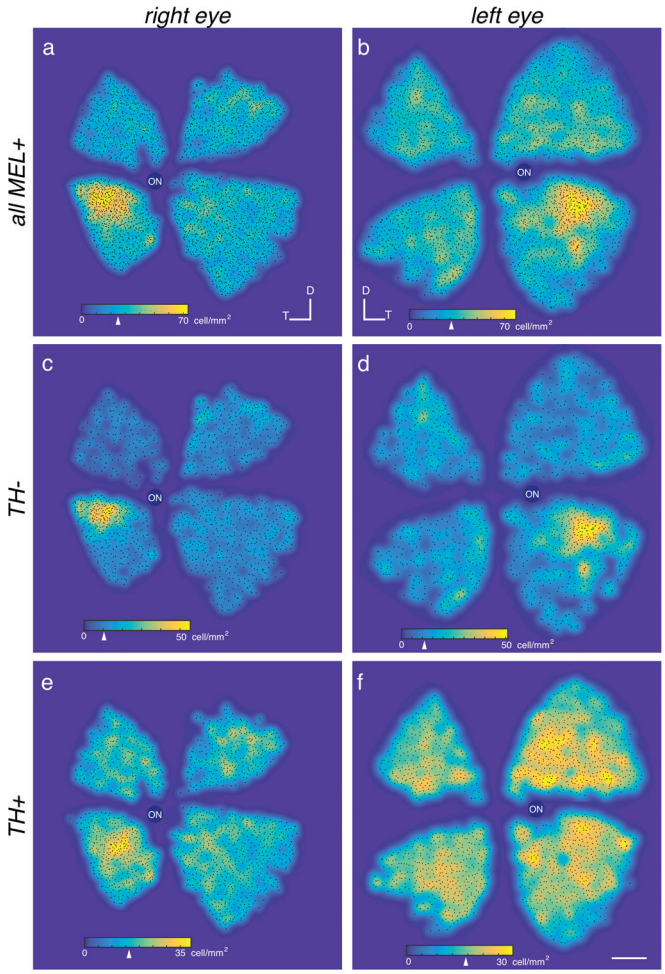

Figure 8.

MEL+ cells exhibit a peak density in the temporal-ventral retina. (a–b) Density maps of all MEL+ cells in right (a) and left (b) eyes from two animals. Arrowhead on colormap scale bars indicate median density. (c–d) Same as (a–b), but for bistratified cells. (e–f) Same as (a–b), but for TH+/MEL+ cells. Scale bar: 2 mm.

Table 1

Primary antibodies

Antibody & RRID	Host animal and Structure of Immunogen	Manufacturer: Catalog #	Concentration
AP-2α AB_2313948	Mouse: AP-2α delta N165 (DNA binding motif) [PMID: 2010091]. Sequence SYMNPGDQSPADSNKTLEKC.	Developmental Studies Hybridoma Bank 3B5	1:500
Brn3a AB_94166	Mouse: Amino Acids 186–224 fused to T7 gene protein.	EMD Millipore: MAB1585	1:1000
ChAT AB_90650	Goat: Human placental enzyme	EMD Millipore: AB144P	1:500
GABA AB_477652	Rabbit	Sigma-Aldrich: A2052	1:1000
GAD-67 AB_2278725	Mouse:Recombinant GAD67 protein	EMD Millipore: MAB5406	1:1000
Melanopsin AB_2156044	Rabbit: Synthetic peptide, corresp. to E(455) QKSKTPKTKRHLPSLDRRM (474) of rat melanopsin	Thermo Fisher: PA1-781	1:1000
RBPMS AB_2492225	Rabbit: Synthetic peptide corresp. to amino acid residues from the N-terminal region of the rat RBPMS sequence conjugated to KLH	PhosphoSolutions: 1830-RBPMS	1:250
RBPMS N.A.	Guinea pig: RBPMS 4–24 with N-terinal cys; GGKAEKENTPSEANLQEEEVRC-KLH CONJUGATE	Dr. Nicholas Brecha, UCLA	1:1000
Tyrosine hydroxylase AB_152435	Chicken: Two synthetic peptide/keyhole limpet hemocyanin (KLH) conjugates. Synthetic peptides corresponded to different regions of the Tyrosine Hydroxylase gene product, but were shared between the human(P07101) and Mouse (P24529) sequences.	Abcam: AB76442	1:1000
Tyrosine Hydroxylase AB_2201528	Mouse: N-terminus directed, monoclonal.	EMD Millipore: MAB318	1:1000

Table 2

Secondary antibodies

Target animal	Emission peak (nm)	Cat. # (Jackson ImmunoResearch): RRID
Mouse	519	715-546-150: AB_2340849
Mouse	667	715-606-150: AB_2340865
Mouse	570	715-166-150: AB_2340816
Guinea pig	519	706-545-148: AB_2340472
Guinea pig	667	706-605-148: AB_2340476
Guinea pig	421	706-475-148: AB_2340470
Rabbit	519	711-545-152: AB_2313584
Rabbit	667	711-605-152: AB_2492288
Chicken	519	703-545-155: AB_2340375
Goat	570	705-16-47: AB_2307351